

# Designing a radiative antidote to CO<sub>2</sub>

Jacob T. Seeley<sup>1</sup>, Nicholas J. Lutsko<sup>2</sup>, David W. Keith<sup>3</sup>

<sup>1</sup>Harvard University Center for the Environment

<sup>2</sup>Scripps Institution of Oceanography

<sup>3</sup>John A. Paulson School of Engineering and Applied Sciences (SEAS), Harvard Kennedy School, Harvard University

## Key Points:

- Conventional, spectrally-flat solar geoengineering strongly suppresses precipitation.
- A spectrally-tuned sunshade restores temperature and rainfall simultaneously in an idealized model.
- Emerging technologies could scatter sunlight in the near-infrared, providing a spectral sunshade.

---

Corresponding author: Jacob T. Seeley, [jacob.t.seeley@gmail.com](mailto:jacob.t.seeley@gmail.com)

## Abstract

Previous results indicate that the global hydrological cycle is more sensitive to Solar Radiation Modification (SRM) than is the surface temperature. Thus, it is expected that restoring temperature with SRM would decrease evaporation and precipitation. However, here we show that a more complete radiative antidote to CO<sub>2</sub> can be obtained by spectrally tuning the SRM intervention, reducing insolation at some wavelengths more than others. By concentrating solar dimming at near-infrared wavelengths, where H<sub>2</sub>O has strong absorption bands, the direct effect of CO<sub>2</sub> on the tropospheric energy budget can be offset, which minimizes perturbations to the hydrological cycle. Idealized cloud-resolving simulations of radiative-convective equilibrium confirm that spectrally-tuned SRM can simultaneously maintain surface temperature and precipitation at their unperturbed values even as large quantities of CO<sub>2</sub> are added to the atmosphere. These results illuminate the connection between the spectral properties of SRM interventions and their potential impacts on precipitation.

## Plain Language Summary

It may be possible to partly counteract CO<sub>2</sub>-driven climate change by solar radiation modification (SRM) that intentionally reduces the amount of sunlight absorbed by the Earth. But different wavelengths of the solar spectrum are absorbed at different altitudes within the surface-atmosphere system, so different climatic effects would be expected depending on which wavelengths of sunlight are affected by an SRM intervention. Here we show that if the goal is to minimize perturbations to the hydrological cycle, the ideal spectrally-tuned SRM intervention focuses on near-infrared wavelengths. Science and policy analysis of SRM has assumed that SRM necessarily entails unwanted changes to precipitation, but we show that if SRM is spectrally-tuned, it may be possible to simultaneously restore global average temperature and precipitation.

## 1 Introduction

Solar radiation Modification (SRM) proposals aim to counteract CO<sub>2</sub>-driven climate change by reducing the amount of sunlight absorbed by the Earth (D. Keith, 2013). Although significant scientific, practical, and ethical questions remain (e.g., P. J. Irvine et al., 2016; Preston, 2013), a growing body of evidence supports the notion that SRM could reduce many climatic changes that normally accompany a rise in CO<sub>2</sub> (e.g., Govin-

dasamy & Caldeira, 2000; P. Irvine et al., 2019). Yet the interventions proposed for SRM do not exactly counteract the radiative impacts of CO<sub>2</sub> forcing, so SRM would not exactly offset CO<sub>2</sub>-driven climate change. For example, a robust feature identified in simulations of geo-engineered climates is a weakened global hydrological cycle (Kravitz, Caldeira, et al., 2013). That is, simulations of climates with high CO<sub>2</sub> and a dimmer sun have lower mean precipitation and evaporation than do unperturbed climates with the same global-mean temperature but lower CO<sub>2</sub> and a brighter sun (e.g., Bala et al., 2008; Tilmes et al., 2013; Smyth et al., 2017).

The cause of the damped hydrological cycle in geo-engineered climates is well understood in terms of atmospheric energetics (e.g., Bala et al., 2008; Kravitz, Rasch, et al., 2013; Kleidon et al., 2015). All else being equal, adding CO<sub>2</sub> to the atmosphere reduces the longwave (LW) cooling of the troposphere, and since the radiative cooling of the troposphere is balanced primarily by latent heat released in precipitating clouds, a reduction in radiative cooling leads to a reduction in precipitation (e.g. Allen & Ingram, 2002; Andrews et al., 2010). This is one of the “direct effects” of CO<sub>2</sub>, so-called because they are not mediated by changes in surface temperature (Dinh & Fueglistaler, 2017; Roms, 2020). Since the direct effect of CO<sub>2</sub> on tropospheric radiative cooling has remained largely uncompensated in the SRM interventions that have been modeled so far, reductions in mean precipitation have been identified as a robust feature of geo-engineered climates (Kravitz, Caldeira, et al., 2013).

But, is this reduction in precipitation really an inevitable outcome of SRM interventions? The purpose of this study is to demonstrate, theoretically and in the context of an idealized model, the possibility of a more complete radiative antidote to CO<sub>2</sub> forcing — an antidote that simultaneously maintains temperature and precipitation at their unperturbed values even as CO<sub>2</sub> is added to the atmosphere. Our approach exploits the fact that the shortwave (SW) opacity of the troposphere is not evenly distributed across the solar spectrum, which means that different wavelengths of sunlight deposit their energy within different layers of the coupled surface-troposphere system (Haigh et al., 2010). This allows a spectrally-tuned SRM intervention (i.e., a wavelength-dependent reduction in insolation) to restore energy balance at the tropopause and at the surface simultaneously. As a result, spectrally-selective SRM can be substantially less disruptive to the hydrological cycle than spectrally-uniform SRM, which is the style of intervention that has been modelled by the majority of previous studies (e.g., the “G1” experiment

from the recent GeoMIP project; Kravitz et al., 2011). While our focus is on an idealized model, we review progress toward achieving spectrally-selective SRM in the real world, and note that the methods and physical insight gained from our approach are relevant to all SRM because no SRM intervention would be exactly spectrally uniform.

## 2 Theory

The use of SRM interventions to counteract CO<sub>2</sub> forcing is motivated by the standard forcing-feedback framework for temperature change (e.g., S. C. Sherwood et al., 2015), which states that the equilibrium change in surface temperature,  $\Delta T_s$ , produced by an external perturbation is proportional to the radiative forcing at the tropopause produced by that perturbation,  $F_t$  (W/m<sup>2</sup>):

$$\Delta T_s = \alpha_T F_t, \quad (1)$$

where the constant of proportionality  $\alpha_T$  (K/W/m<sup>2</sup>) is known as the “climate sensitivity” parameter. In this context, radiative forcing refers to the change in net radiative flux produced by the perturbation itself (i.e., before any adjustments in surface temperature). Motivated by equation (1), the SRM interventions previously modeled in the literature have aimed to lessen CO<sub>2</sub>-induced warming by offsetting the (positive) CO<sub>2</sub> radiative forcing at the tropopause with a countervailing (negative) radiative forcing at the tropopause from SRM.

While the energy budget at the tropopause controls changes in surface temperature, it alone does not constrain the precipitation rate because changes in precipitation  $\Delta P$  (kg/m<sup>2</sup>/s) are driven by changes in *tropospheric* radiative cooling,  $\Delta Q$  (W/m<sup>2</sup>):

$$\Delta P = -\alpha_P \Delta Q, \quad (2)$$

where  $\alpha_P$  (kg/J) is a “hydrological sensitivity” parameter<sup>1</sup> (e.g., O’Gorman et al., 2011; Pendergrass & Hartmann, 2014), and where negative values of  $Q$  indicate the typical situation of net tropospheric radiative cooling. Since tropospheric radiative cooling depends on surface temperature as well as external perturbations such as increased CO<sub>2</sub> or changes in insolation, it is useful to separate  $\Delta Q$  into the component produced by external perturbations and the component that depends explicitly on  $\Delta T_s$  (Lambert & Faull, 2007):

$$\Delta Q = F_a + \frac{\partial Q}{\partial T_s} \Delta T_s. \quad (3)$$

---

<sup>1</sup> Note that others have defined the hydrological sensitivity as  $\Delta P/\Delta T_s$  (e.g., Kleidon et al., 2015).

Here the external perturbation component  $F_a$  can be regarded as a radiative forcing of the troposphere, which is simply the difference between the radiative forcing of the external perturbation evaluated at the tropopause and at the surface:

$$F_a = F_t - F_s. \quad (4)$$

From equations (1–4), we can deduce that a “radiative antidote” to  $\text{CO}_2$  that maintains  $\Delta T_s = \Delta P \simeq 0$  must offset the  $\text{CO}_2$  radiative forcing at the tropopause and at the surface simultaneously.

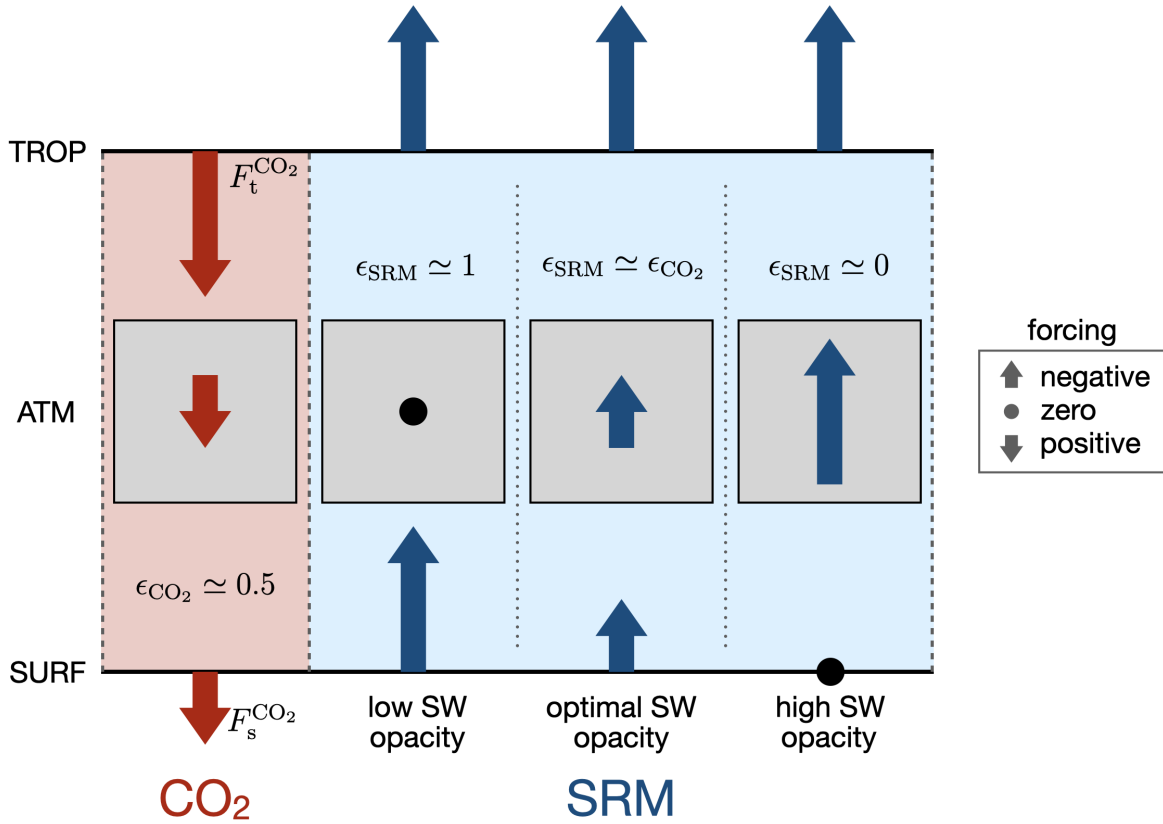


**Figure 1.** A schematic depiction of the radiative forcings at the tropopause (TROP), surface (SURF), and within the troposphere (ATM) produced by increasing  $\text{CO}_2$  (leftmost column), or by idealized “sunshade” SRM interventions (three columns at right) in the style of the G1 experiment from GeoMIP (Kravitz et al., 2011). The SRM case is split into three sub-cases with bulk tropospheric shortwave opacities increasing from left to right. For a given perturbation  $x$ ,  $\epsilon_x$  is the ratio between the associated radiative forcing at the surface and at the tropopause:

$$\epsilon_x \equiv F_s^x / F_t^x.$$

Is such a radiative antidote to CO<sub>2</sub> possible? The left column of Figure 1 shows a schematic depiction of the radiative forcings produced by increased CO<sub>2</sub>: a positive forcing at the tropopause  $F_t^{\text{CO}_2}$ , and a smaller positive forcing at the surface  $F_s^{\text{CO}_2}$ . For a given perturbation  $x$ , it is convenient to define a measure of how suppressed the associated radiative forcing is at the surface compared to at the tropopause:

$$\epsilon_x \equiv F_s^x / F_t^x. \quad (5)$$

For example, for a CO<sub>2</sub> perturbation, the global-mean surface forcing is about half as large as the global-mean tropopause forcing (i.e.,  $\epsilon_{\text{CO}_2} \simeq 0.5$ ; Huang et al., 2017).

How do the surface and tropopause forcings compare for SRM interventions? The answer depends on 1) the shortwave opacity of the troposphere, and 2) the spectral signature of the SRM intervention. The most commonly-studied SRM intervention is the idealized “sunshade” experiment (“G1”) from the GeoMIP protocol (Kravitz et al., 2011). This experiment calls for a simple reduction in the solar constant, which is implemented in numerical models as a spectrally-uniform fractional reduction in downwelling short-wave at the top-of-atmosphere (TOA). For this style of spectrally-flat SRM,  $\epsilon_{\text{SRM}}$  depends on the bulk shortwave opacity of the troposphere: for a troposphere that is completely (i.e., at all wavelengths) transparent to sunlight,  $F_t^{\text{SRM}} = F_s^{\text{SRM}}$  and  $\epsilon_{\text{SRM}} = 1$ , whereas for a troposphere that is completely opaque to sunlight,  $F_t^{\text{SRM}}$  is finite while  $F_s^{\text{SRM}} = 0$ , and so  $\epsilon_{\text{SRM}} = 0$  (Figure 1, columns 2 and 4).

The above considerations allow us to understand what happens to the hydrological cycle when a CO<sub>2</sub> perturbation is combined with a sunshade-type SRM intervention. Combining equations (1–5), and setting  $F_t^{\text{CO}_2} = -F_t^{\text{SRM}}$  as specified by the G1 GeoMIP protocol, we obtain the following expression for the change in precipitation:

$$\Delta P = \alpha_P F_t^{\text{CO}_2} (\epsilon_{\text{CO}_2} - \epsilon_{\text{SRM}}). \quad (6)$$

Hence the only circumstance in which spectrally-flat SRM can counteract CO<sub>2</sub> forcing at the tropopause and at the surface simultaneously is if the troposphere happens to have the correct intermediate bulk shortwave opacity so that  $\epsilon_{\text{SRM}} = \epsilon_{\text{CO}_2}$ . Otherwise, if a spectrally-flat SRM intervention is scaled such that  $F_t^{\text{SRM}}$  completely counteracts  $F_t^{\text{CO}_2}$ , there will be a residual radiative forcing of the troposphere. This residual forcing will drive a change in convective enthalpy fluxes from the surface (e.g., Dinh & Fueglistaler, 2017), and perturb the hydrological cycle according to equations (2–3), as has been observed in the GeoMIP G1 experiment (Kravitz, Caldeira, et al., 2013; Tilmes et al., 2013).

From the fact that the G1 experiment has yielded *reduced* mean precipitation (i.e.,  $\Delta Q > 0$ ), we can deduce that the bulk shortwave opacity of Earth's contemporary troposphere is too low (i.e.,  $\epsilon_{\text{SRM}} > \epsilon_{\text{CO}_2}$ ) for a spectrally-flat solar dimming to offset the direct effect of  $\text{CO}_2$  on tropospheric radiative cooling. By contrast, a spectrally-tuned SRM intervention could, in principle, concentrate the solar dimming in a portion of the solar spectrum with above-average tropospheric shortwave opacity, thereby allowing  $\epsilon_{\text{SRM}} \simeq \epsilon_{\text{CO}_2}$  by construction. This is the basic insight underlying our suggestion that spectrally-tuned solar dimming could be a more complete radiative antidote to  $\text{CO}_2$  forcing.

To quantitatively explore the potential of spectrally-tuned solar dimming, let us split the downwelling shortwave radiation at the tropopause,  $S_t^\downarrow$ , into  $N$  bands indexed by  $i$ , each with incoming power  $S_i$  ( $\text{W}/\text{m}^2$ ):

$$S_t^\downarrow = \sum_{i=1}^N S_i \quad (7)$$

In each of these bands, we denote the tropospheric transmissivity to vertically-propagating radiation as  $\mathcal{T}_i = e^{-\tau_i}$ , where  $\tau_i$  is the total tropospheric column SW optical depth<sup>2</sup> in band  $i$  (assumed to be uniform within the band). If  $S_i$  is reduced by some fraction, the ratio of the associated forcings at the surface and tropopause is found, via Beer's law, to be

$$\epsilon_i = \frac{\mathcal{T}_i^{1/\bar{\mu}}(1 - a_i)}{1 - a_i \mathcal{T}_i^{1/\bar{\mu} + D}}, \quad (8)$$

where  $\bar{\mu}$  is the effective cosine of the solar zenith angle,  $D = 1.5$  is a two-stream hemispheric diffusivity factor (Clough et al., 1992), and where we have assumed a Lambertian surface with a band-specific SW albedo  $a_i$ . The optimal shortwave optical depth  $\tau^*$  for offsetting  $\text{CO}_2$  forcing is found by setting  $\epsilon_i$  as given by equation (8) equal to  $\epsilon_{\text{CO}_2}$ . To get a rough sense of the numbers, we can take  $\epsilon_{\text{CO}_2} = 0.5$  and  $a_i = 0$ , yielding

$$\tau^* = \bar{\mu} \ln(2) \simeq 0.46, \quad (9)$$

where we have assumed  $\bar{\mu} = 2/3$  (as is appropriate for the global mean; Cronin, 2014). For  $a_i \neq 0$ ,  $\tau^*$  is easily obtained via a rootsolver.

Now suppose we reduce the downwelling SW at the tropopause by band-specific fractional amounts  $\gamma_i$ , for  $0 \leq \gamma_i \leq 1$  ( $\gamma_i = 0$  corresponds to no reduction at the tropopause,

---

<sup>2</sup> For simplicity, here we assume SW attenuation is due only to molecular absorption, which is true for clear skies at wavelengths where Rayleigh scattering is negligible (e.g., the near-infrared).

whereas  $\gamma_i = 1$  corresponds to complete blocking). The challenge of spectrally-tuned solar dimming amounts to finding a set of  $\gamma_i$  (i.e., a spectral filter) that simultaneously offsets  $F_t^{\text{CO}_2}$  and  $F_s^{\text{CO}_2}$ , which is equivalent to simultaneously solving the following two equations:

$$F_t^{\text{CO}_2} = \sum_{i=1}^N \gamma_i S_i (1 - a_i \mathcal{T}_i^{1/\bar{\mu}+D}), \quad (10)$$

$$F_s^{\text{CO}_2} = \sum_{i=1}^N \gamma_i S_i \mathcal{T}_i^{1/\bar{\mu}} (1 - a_i). \quad (11)$$

To that end, it is instructive to consider a few limiting cases:

1. Filtering a band that passes through the atmosphere unabsorbed ( $\mathcal{T}_i = 1$ ) perturbs the tropopause and surface energy budgets by the same amount,  $\gamma_i S_i (1 - a)$ .
2. Filtering a band that is completely absorbed in the troposphere ( $\mathcal{T}_i = 0$ ) perturbs the tropopause energy budget by  $\gamma_i S_i$ , while leaving the surface energy budget unaffected.
3. Filtering a band for which  $\mathcal{T}_i^{1/\bar{\mu}} (1 - a) / [1 - a \mathcal{T}_i^{1/\bar{\mu}+D}] = \epsilon_{\text{CO}_2}$  offsets the same fraction of  $\text{CO}_2$  forcing at the tropopause and at the surface.

These principles suggest that there are many equally valid algorithms that could be used to design a spectral SRM filter. For simplicity, in this work we will simply find a contiguous band of wavenumbers that happens to have the correct distribution of optical depths to simultaneously solve (10–11).

### 3 Experimental methods

Our understanding of the effect of SRM on global-mean precipitation is based on a radiative-convective equilibrium (RCE) perspective on the tropospheric energy budget (Bala et al., 2008; Kravitz, Rasch, et al., 2013; Kleidon et al., 2015). The state of RCE is the simplest system that faithfully captures the vertically-resolved energy budget of Earth’s troposphere — that is, the balance between radiative cooling and convective heating. Therefore, the RCE framework is a natural testbed for a proof-of-principal demonstration of spectral SRM. We conducted RCE simulations with the cloud-resolving model DAM (Romps, 2008), which has been used extensively to study tropical convection in Earth’s atmosphere (e.g., Romps & Kuang, 2010; Romps, 2011, 2014; Seeley & Romps, 2015, 2016; Seeley, Jeevanjee, Langhans, & Romps, 2019; Seeley, Jeevanjee, & Romps,



2019). The default radiation scheme in DAM is RRTM (Clough et al., 2005; Iacono et al., 2008), a correlated- $k$  code, but for the purpose of this study we have coupled DAM to a clear-sky radiation scheme that simply integrates the radiative transfer equation on a user-supplied spectral grid using standard molecular opacity data from the HITRAN database (Gordon et al., 2017). This “brute-force” (i.e., wavenumber-by-wavenumber) approach to radiation greatly facilitates the investigation of spectrally-tuned solar dimming, without meaningful reductions in accuracy. We have benchmarked our radiation scheme against RRTM and a line-by-line radiation code for an appropriate range of clear-sky conditions and find very good agreement (Figures S2-3). In addition, whereas DAM typically uses the Lin-Lord-Krueger bulk microphysics scheme (Lin et al., 1983; Lord et al., 1984; Krueger et al., 1995), for this study we use the simplified cloud microphysics parameterization described in Seeley, Jeevanjee, & Romps (2019). Since we adopt a clear-sky perspective here, our results are not sensitive to the microphysics scheme, and we believe that the simplified treatment of microphysics is appropriate for the present study, which is intended simply as a proof-of-principle. For further details regarding the numerical modelling configuration, see the Supporting Information.

We first ran a control experiment (referred to as “CTRL”) with a total solar irradiance (TSI) of  $510.375 \text{ W/m}^2$  and a fixed cosine of the solar zenith angle of  $\bar{\mu} = 2/3$  (Cronin, 2014), yielding a downwelling shortwave flux at the TOA of  $340.25 \text{ W/m}^2$ ; this value matches the planetary-mean insolation  $S_0/4$ , where  $S_0 = 1361 \text{ W/m}^2$  is the solar constant. The CTRL simulation was specified to have a preindustrial  $\text{CO}_2$  concentration of 280 ppm and no ozone. CTRL was initialized from a similar RCE simulation over a fixed sea surface temperature and run for 1 year over a slab-ocean surface with a wavelength-independent albedo of 0.285, infinite horizontal conductivity (i.e., a uniform temperature), and heat capacity equivalent to a layer of liquid water of depth 20 cm. Results for CTRL were averaged over the final 200 days of model time. The equilibrated state of CTRL has a slab-ocean temperature of 288.64 K and mean precipitation rate of 3.17 mm/day. We then branched three experiments from the equilibrated state of CTRL: an abrupt quadrupling of  $\text{CO}_2$  (referred to as “ $4\times\text{CO}_2$ ”), and two experiments for which the  $\text{CO}_2$  quadrupling was accompanied by the application of some type of SRM. These branched simulations were run for an additional 3 years of model time, with results averaged over the final 100 days.

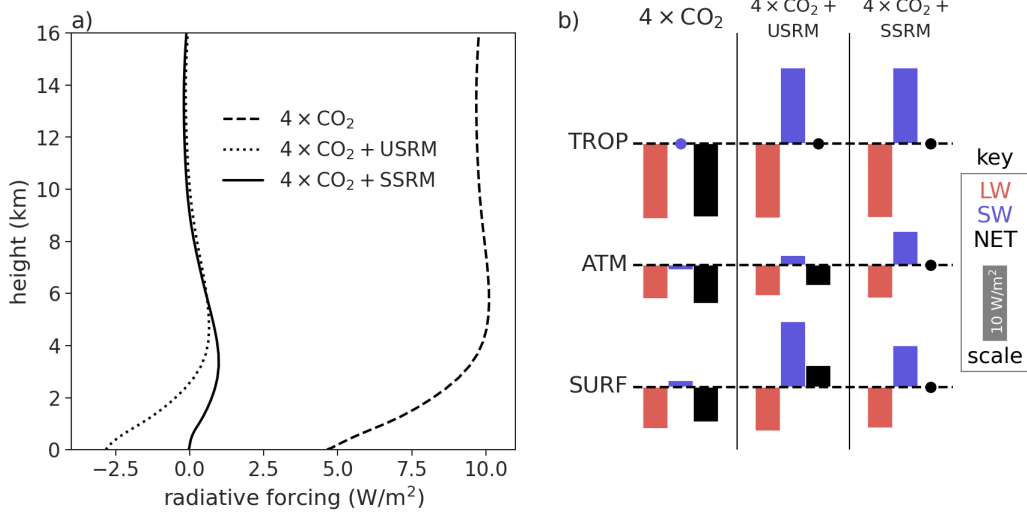


**Figure 2.** (a) Vertically-resolved radiative forcings, diagnosed as differences in net radiative fluxes. The forcings are shown for the three branched simulations with quadrupled CO<sub>2</sub>, two of which also include an SRM interventions (USRM or SSRM) as described in the main text. (b) Radiative forcings evaluated at the tropopause (top row, TROP;  $z \simeq 15$  km), surface (bottom row, SURF), and within the troposphere (middle row, ATM = TROP - SURF). For each simulation and level, the longwave (LW), shortwave (SW), and net (LW+SW) forcings are color-coded. By convention, positive forcings are depicted as downward-pointing bars, with the scale indicated by the gray 10 W/m<sup>2</sup> bar shown in the key; forcings with magnitude less than 0.2 W/m<sup>2</sup> are depicted as filled circles.

The SRM interventions were designed according to the principles discussed in section 2. We first calculated the instantaneous radiative forcing from a quadrupling of CO<sub>2</sub> by double-calling the radiative transfer scheme at every radiative time step of the CTRL simulation (once with 280 ppm CO<sub>2</sub> and once with 1120 ppm CO<sub>2</sub>), and taking the difference between the net radiative fluxes. We evaluated these forcings at the tropopause and at the surface; the tropopause was identified as the level at the top of the troposphere where the time-averaged cloud fraction in CTRL falls below 1% (an altitude of approximately 15 km). For the CO<sub>2</sub> quadrupling, the instantaneous radiative forcing at the tropopause was found to be  $F_t = 9.71$  W/m<sup>2</sup>, while the forcing at the surface was  $F_s = 4.63$  W/m<sup>2</sup> (Fig. 2; see also Table 1). Note that this implies  $\epsilon_{\text{CO}_2} \simeq 0.5$  in our CTRL experiment, close to the global-mean value reported in the literature (Huang et al., 2017). Strictly speaking, the forcing  $F_t$  that enters into the forcing-feedback framework of equation (1)

237 should be the so-called *adjusted* forcing, which is the radiative flux imbalance at the tropopause  
 238 after stratospheric temperatures adjust to return the stratosphere to radiative equilib-  
 239 rium (e.g., Smith et al., 2018). For simplicity, here we use the instantaneous forcing in  
 240 place of the adjusted forcing, which was not found to be a large source of error.

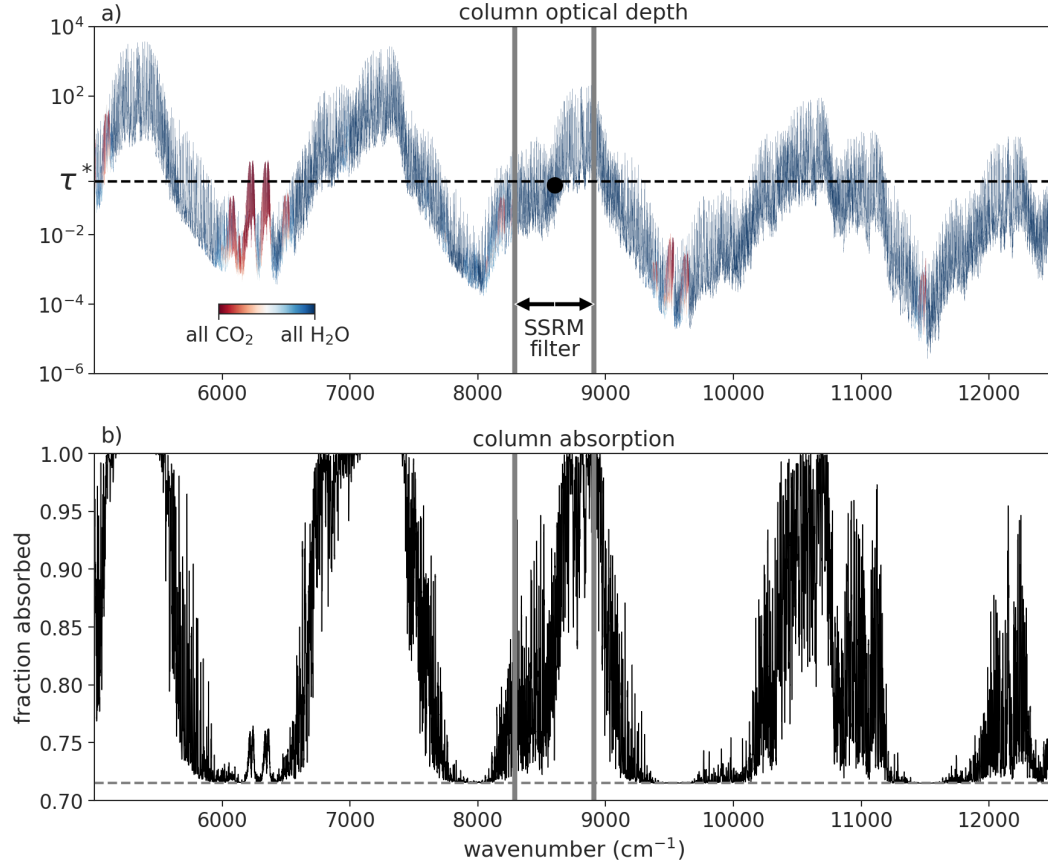


**Figure 3.** (a) Spectrally-resolved column optical depth from the CTRL experiment in the near-infrared. The data is color-coded according to the fraction of the surface optical depth contributed by H<sub>2</sub>O versus CO<sub>2</sub>. The optimal optical depth for offsetting CO<sub>2</sub> forcing at the tropopause and surface simultaneously,  $\tau^*$ , is indicated by the horizontal dashed line. The spectral SRM filter spans the wavenumber range 8290–8910 cm<sup>-1</sup> and is indicated by the gray bars. The (geometric) mean optical depth within the filtered band is indicated by the filled circle. (b) Spectrally-resolved column absorption from CTRL in the near-infrared. The surface co-albedo (i.e., 1 minus the surface albedo) is plotted as the horizontal dashed line, and sets the minimum column absorption (i.e., for a transparent atmosphere).

In accordance with the GeoMIP G1 experiment (Kravitz et al., 2011), our first SRM intervention was designed to completely offset the CO<sub>2</sub> radiative forcing at the tropopause by reducing the solar constant. Since this amounts to a spectrally-uniform reduction in TOA downwelling shortwave, we will refer to this intervention as USRM (with the “U” indicating that this intervention is spectrally-uniform). The net shortwave flux at the tropopause in CTRL is  $S_t = 259.0 \text{ W/m}^2$ , so we reduced the TSI by the factor  $F_t/S_t = 3.75\%$  (from  $510.375 \text{ W/m}^2$  to  $491.23 \text{ W/m}^2$ ). To assess the efficacy of the intervention, we averaged the radiative fluxes over the first week of the branched simulation, and calculated radiative forcings as differences between these radiative fluxes and the mean radiative fluxes from CTRL. As can be seen in the middle column of Figure 2b ( $4\times\text{CO}_2+\text{USRM}$ ), this spectrally-uniform SRM intervention restores the energy budget at the tropopause (i.e., there is a negligible difference in net radiative flux at the tropopause between CTRL and  $4\times\text{CO}_2+\text{USRM}$ ), due to a cancellation between the positive LW forcing from the CO<sub>2</sub> perturbation and the negative SW forcing of the SRM intervention. However, there is a net forcing of the surface for this intervention, and equivalently, a change to the bulk radiative flux divergence of the troposphere. The perturbation to the bulk tropospheric radiative heating is positive (i.e., an anomalous heating) with magnitude  $+2.72 \text{ W/m}^2$ . The LW effect of the CO<sub>2</sub> perturbation on the radiative cooling of the atmosphere is slightly larger than this, but is partially offset by a small anomalous shortwave cooling due to the USRM intervention.

The goal of spectrally-tuned solar dimming, on the other hand, is to *completely* offset the direct effect of CO<sub>2</sub> by producing a larger anomalous shortwave cooling of the troposphere. Here we suggest that this can be accomplished by concentrating the solar dimming in the near-infrared wavelengths (roughly  $5000\text{--}12500 \text{ cm}^{-1}$ ), where H<sub>2</sub>O has strong absorption bands that are primarily responsible for the shortwave heating of the troposphere. Specifically, to ensure a quantitatively accurate filter, we must choose  $\gamma_i$  to satisfy equations 10–11. By trial and error, we found that setting  $\gamma_i = 1$  in the wavenumber range  $8290\text{--}8910 \text{ cm}^{-1}$  accomplishes this goal (Fig. 3). Note that the opacity in this band is attributable almost entirely to H<sub>2</sub>O. There are other filters that also satisfy equations 10–11, but we will take the filter shown in Figure 3 as our example of spectrally-tuned SRM (SSRM). The third column in Figure 2b shows that this filter, when combined with a quadrupling of CO<sub>2</sub>, produces no net forcing at the tropopause *or* surface, and therefore no anomalous bulk radiative heating of the troposphere. The filter works

because it contains the correct balance of optically-thin and optically-thick wavelengths: although the optical depths within this band span roughly 4 orders of magnitude, the (geometric) mean optical depth within the filtered band is very close to the optimal optical depth  $\tau^* = 0.34$  calculated by setting the right-hand side of equation (8) equal to  $\epsilon_{\text{CO}_2}$  and solving for  $\tau_i$  (Fig. 3a). The most optically-thick wavelengths within the filtered band are almost entirely absorbed within the troposphere, whereas the most optically-thin wavelengths are absorbed only at the surface (Fig. 3b).

Although the SSRM filter nullifies the direct effect of  $\text{CO}_2$  on *bulk* tropospheric radiative heating, the vertically-resolved compensation is not exact (Fig. 3a). This slight redistribution of radiative heating rates in the vertical could, in principle, affect atmospheric dynamics.

## 4 Results

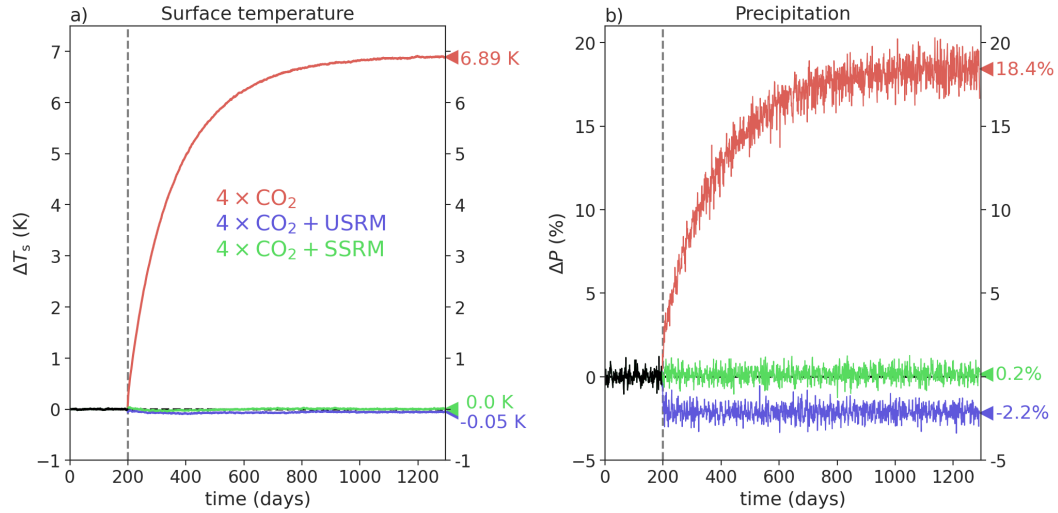


**Figure 4.** Anomaly timeseries of (a) slab-ocean temperature  $T_s$  and (b) precipitation rate  $P$  from the DAM experiments. The three experiments with quadrupled  $\text{CO}_2$  are branched from CTRL at day 200 and run for 3 additional years of model time. The precipitation timeseries is plotted as a moving average with a centered window of 1 week to reduce noise. Quantities averaged over the final 100 days of the simulations are marked on the ordinates at right.

We have seen in Figures 2-3 that it is possible to design a spectrally-tuned SRM intervention that offsets the radiative forcing from  $\text{CO}_2$  at the tropopause and at the surface simultaneously. But, does this SSRM approach outperform the USRM approach at

	4×CO <sub>2</sub>	4×CO <sub>2</sub> +USRM	4×CO <sub>2</sub> +SSRM
$F_t$ (W/m <sup>2</sup> )	9.71	-0.105	-0.155
$F_s$ (W/m <sup>2</sup> )	4.63	-2.82	-0.04
$\Delta T_s$ (K)	6.89	-0.055	0.005
$\Delta P$ (%)	18.4	-2.16	0.157

**Table 1.** Radiative forcings at the tropopause ( $F_t$ ) and surface ( $F_s$ ), as well as mean changes in surface temperature  $T_s$  and precipitation  $P$ , from the three DAM experiments with quadrupled CO<sub>2</sub>.

the task of maintaining temperature and precipitation at their unperturbed values? Figure 4 shows time series of surface temperature and precipitation from the branched RCE experiments. The surface warms rapidly in the 4×CO<sub>2</sub> experiment, eventually equilibrating at a surface temperature warmer by  $\Delta T_s = 6.89$  K after approximately 3 years of model time. Therefore, the equilibrium climate sensitivity for our model configuration is approximately 3.5 K, squarely within the best-estimate range for ECS (S. Sherwood et al., 2020). This large warming causes an increase in mean precipitation of 18.4%, or roughly 2.7 %/K, which is the expected effect of a deepening troposphere under warming (Jeevanjee & Romps, 2018).

Both SRM interventions (USRM and SSRM) greatly reduce the magnitude of changes to temperature and precipitation. For surface temperature, the two interventions are roughly equally effective: both limit changes in surface temperature to  $\leq 0.05$  K, more than two orders of magnitude smaller than the warming caused by quadrupling CO<sub>2</sub> without any form of SRM. For precipitation, however, the effectiveness of the SRM interventions differs greatly: USRM causes a decrease in precipitation of -2.2%, whereas SSRM limits the change in precipitation to less than +0.2%. Therefore, the SSRM intervention is indeed a more complete radiative antidote to CO<sub>2</sub> forcing than the USRM intervention, because it nullifies both the greenhouse effect of CO<sub>2</sub> on surface temperature and the direct effect of CO<sub>2</sub> on precipitation. These results are summarized in Table 1.

## 5 Discussion

In this study, we have developed the theory of spectrally-tuned SRM interventions. Such interventions have the goal of simultaneously maintaining surface temperature and

precipitation at their unperturbed values even as large quantities of CO<sub>2</sub> are added to the atmosphere. Theoretically, this is made possible by the strong absorption bands of H<sub>2</sub>O in the near-infrared: by concentrating solar dimming at these wavelengths, it is possible to produce an anomalous shortwave cooling of the troposphere that offsets the long-wave heating of additional CO<sub>2</sub>. Equivalently, a successful spectrally-tuned solar dimming preserves the energy budget of the tropopause and the surface (equations 10–11), whereas spectrally-flat solar dimming can preserve the energy budget at the tropopause but leaves the surface energy budget perturbed.

As a proof-of-principle, we have demonstrated the success of spectrally-tuned SRM in idealized cloud-resolving model experiments. Although we have only investigated SSRM in a configuration that entirely offsets CO<sub>2</sub> forcing at the tropopause (in accordance with the GeoMIP G1 protocol; Kravitz et al., 2011), our results can be generalized to help understand the effects of SRM interventions that offset only a fraction of CO<sub>2</sub> forcing. Suppose that an SRM intervention is designed such that  $F_t^{\text{SRM}} = -\beta F_t^{\text{CO}_2}$ , for  $0 \leq \beta \leq 1$  (i.e.,  $\beta = 0$  corresponds to no offsetting of CO<sub>2</sub> forcing, while  $\beta = 1$  corresponds to complete offsetting). Combining equations (1–5), we obtain the following expression for the change in precipitation, which generalizes equation (6):

$$\Delta P = -\alpha_P F_t^{\text{CO}_2} \left[ \underbrace{(1 - \beta) + \beta \epsilon_{\text{SRM}} - \epsilon_{\text{CO}_2}}_{\text{direct effect}} + \underbrace{\frac{\partial Q}{\partial T_s} \alpha_T (1 - \beta)}_{\text{warming effect}} \right], \quad (12)$$

where we have identified with underbraces the two sources of changes in precipitation:

1) the direct effect from the combination of a CO<sub>2</sub> perturbation and an SRM intervention, and 2) the effect of warming on precipitation. By putting in representative numbers, we can use equation (12) to make several useful observations. Consider first CO<sub>2</sub> forcing alone ( $\beta = 0$ ). Taking  $\epsilon_{\text{CO}_2} = 0.5$ ,  $\frac{\partial Q}{\partial T_s} = -3 \text{ W/m}^2/\text{K}$  (Jeevanjee & Romps, 2018), and  $\alpha_T = 0.7 \text{ K/W/m}^2$  (as inferred from our 4×CO<sub>2</sub> experiment, in which a  $\simeq 10 \text{ W/m}^2$  tropopause forcing causes a  $\simeq 7 \text{ K}$  warming), equation (12) suggests that the direct effect of CO<sub>2</sub> on precipitation is smaller than the warming effect by a factor of about 1/4, close to the estimate of Romps (2020). This implies that, if the goal is to minimize disruption to the hydrological cycle, minimizing changes in surface temperature via the tropopause energy budget is the most powerful lever. It is only when  $\beta \simeq 1$ , as in our experiments and the G1 experiment protocol, that the warming effect is suppressed enough to allow the direct effect to dominate changes in precipitation; in this limit, equation (12)

shows that the direct effect is controlled by the difference  $\epsilon_{\text{SRM}} - \epsilon_{\text{CO}_2}$ , as previously discussed in section 2 (c.f. equation 6, Fig. 1). In this limit, the spectral properties of the SRM intervention should be tuned so that  $\epsilon_{\text{SRM}} = \epsilon_{\text{CO}_2}$ , to minimize the perturbation to the precipitation rate.

For intermediate values of  $\beta$  — for example,  $\beta = 0.5$ , as investigated by P. Irvine et al. (2019) — it is not necessarily desirable to set  $\epsilon_{\text{SRM}} = \epsilon_{\text{CO}_2}$ . The reason is that, for  $\beta = 0.5$ , the uncompensated tropopause forcing will cause warming, driving an increase in precipitation. Again, if the goal is to minimize disruption to the hydrological cycle, in this case the direct suppression of precipitation by  $\text{CO}_2$  is desirable, and our SRM intervention should be designed to leave this direct effect as large as possible. The best we can do is to set  $\epsilon_{\text{SRM}} = 1$ , which corresponds to concentrating the solar dimming in a wavenumber band where the atmosphere is completely transparent. This makes sense: in the case with halved warming, precipitation is expected to increase, and any anomalous tropospheric shortwave cooling caused by an SRM intervention acting at non-transparent wavelengths will push the precipitation rate further from its unperturbed state. The conclusion is that the optimal spectral properties of an SRM intervention depend on the magnitude of the intervention. Lutsko et al. (2020) reached a similar conclusion regarding the optimal latitudinal profile of SRM forcing.

Given the success of spectral SRM in our idealized model, it is natural to wonder how spectral SRM might be realized in the real world. At present, there is no off-the-shelf commercial technology that could be used to implement spectral SRM without prohibitive costs and environmental impacts. Yet, SRM would likely be implemented over a time scale of a century or more, so there is time for technological innovation, and already there are signs that “designer materials” with tuneable extinction coefficients at near-infrared wavelengths may be within reach. Metallic nanoparticles that exhibit optical plasmonic resonance (Khlebtsov & Dykman, 2010) can exhibit narrow-band scattering or absorption in the optical and near-infrared, with resonant spectral widths of order 1000 wavenumbers (Berkovitch et al., 2010) — consistent with the size of filter we analyze in this work. Diffractive structures and resonant scatterers for SRM were proposed over two decades ago (Teller et al., 1997); similarly, self-levitating atmospheric scatterers for SRM were proposed a decade ago (D. W. Keith, 2010), and are now being physically demonstrated in the lab (Cortes et al., 2020). A small but growing body of literature has explored space-based SRM since 1989, and several of these proposals exploit



374 diffractive screens (Angel, 2006). All of these methods could serve as the basis for spectrally-  
 375 tunable SRM interventions.

376 Even if it turns out that spectrally-tuned SRM technologies will never be practi-  
 377 cal or cheap enough for use, our results remain relevant to more mainstream approaches  
 378 to SRM (e.g., with stratospheric sulfate aerosols), for the simple reason that any real-  
 379 world implementation of SRM will not be spectrally uniform. We have shown how to map  
 380 the spectral characteristics of candidate SRM technologies onto their expected impacts  
 381 on precipitation, thereby providing a new metric for evaluating such technologies. In-  
 382 deed, prior work has shown that different SRM technologies have different effects on pre-  
 383 cipitation rates (Niemeier et al., 2013), presumably because of their differing spectral char-  
 384 acteristics. Equations (10–11) provide a quick method of parsing the “design space” of  
 385 SRM technologies without resorting to computationally-expensive simulations with global  
 386 climate models.

387 Overall, although our results regarding the potential of spectral SRM are promis-  
 388 ing, many questions remain. It is important to realize that designing a radiative anti-  
 389 dote to CO<sub>2</sub> is substantially easier for atmospheres that are statistically homogeneous  
 390 in the horizontal (e.g., our RCE simulations). On the real Earth, spatial heterogeneity  
 391 in surface temperature, water vapor content, and albedo would cause the ideal spectral  
 392 SRM intervention itself to be spatially heterogeneous. Another weakness of the theory  
 393 of spectral SRM developed here is that the surface Bowen ratio is unconstrained, which  
 394 means that the precipitation rate could change even when the radiative energy budget  
 395 of the troposphere is unperturbed. This effect could be especially important in models  
 396 with heterogeneous surface conditions. Global models are the only way to assess changes  
 397 to regional precipitation, which are more relevant to society than the global-mean change.  
 398 For these reasons and more, future work should test the effectiveness of spectral SRM  
 399 in comprehensive global models. It seems likely that SRM interventions that are less dis-  
 400 ruptive of the tropospheric energy balance will be less disruptive of the climate on a re-  
 401 gional scale, but further work is needed to verify this hypothesis.

## 402 Acknowledgments

403 Simulation data and Python source code for reproducing the figures in this manuscript  
 404 is available at <https://doi.org/10.5281/zenodo.4035201>.

## References

- Allen, M. R., & Ingram, W. J. (2002, sep). Constraints on future changes in climate and the hydrologic cycle. *Nature*, *419*(6903), 224–32. doi: 10.1038/nature01092
- Andrews, T., Forster, P. M., Boucher, O., Bellouin, N., & Jones, A. (2010). Precipitation, radiative forcing and global temperature change. *Geophysical Research Letters*, *37*(14). doi: 10.1029/2010GL043991
- Angel, R. (2006). Feasibility of cooling the Earth with a cloud of small spacecraft near the inner Langrange point (L1). *Proceedings of the National Academy of Sciences of the United States of America*, *103*(46), 17184–17189. doi: 10.1073/pnas.0608163103
- Bala, G., Duffy, P. B., & Taylor, K. E. (2008). Impact of geoengineering schemes on the global hydrological cycle. *Proceedings of the National Academy of Sciences*, *2008*.
- Berkovitch, N., Ginzburg, P., & Orenstein, M. (2010). Concave plasmonic particles: Broad-band geometrical tunability in the near-infrared. *Nano Letters*, *10*(4), 1405–1408. doi: 10.1021/nl100222k
- Clough, S. A., Iacono, M. J., & Moncet, J.-l. (1992). Line-by-line calculations of atmospheric fluxes and cooling rates: Application to water vapor. *Journal of Geophysical Research*, *97*(D14), 15761.
- Clough, S. A., Shephard, M. W., Mlawer, E. J., Delamere, J. S., Iacono, M. J., Cady-Pereira, K., ... Brown, P. D. (2005). Atmospheric radiative transfer modeling: A summary of the AER codes. *Journal of Quantitative Spectroscopy and Radiative Transfer*, *91*(2), 233–244. doi: 10.1016/j.jqsrt.2004.05.058
- Cortes, J., Stanczak, C., Azadi, M., Narula, M., Nicaise, S. M., Hu, H., & Bargatin, I. (2020). Photophoretic Levitation of Macroscopic Nanocardboard Plates. *Advanced Materials*, *32*(16), 1–7. doi: 10.1002/adma.201906878
- Cronin, T. W. (2014). On the Choice of Average Solar Zenith Angle. *Journal of the Atmospheric Sciences*, *71*(8), 2994–3003. doi: 10.1175/JAS-D-13-0392.1
- Dinh, T., & Fueglistaler, S. (2017). Mechanism of Fast Atmospheric Energetic Equilibration Following Radiative Forcing by CO<sub>2</sub>. *Journal of Advances in Modeling Earth Systems*, *9*(7), 2468–2482. doi: 10.1002/2017MS001116
- Gordon, I. E., Rothman, L. S., Hill, C., Kochanov, R. V., Tan, Y., Bernath, P. F., ... Zak, E. J. (2017). The HITRAN2016 molecular spectroscopic database.

- 438 *Journal of Quantitative Spectroscopy & Radiative Transfer*, 203, 3–69. doi:  
439 10.1016/j.jqsrt.2017.06.038
- 440 Govindasamy, B., & Caldeira, K. (2000). Geoengineering Earth’s radiation balance  
441 to mitigate CO<sub>2</sub>-induced climate change. *Geophysical Research Letters*, 27(14),  
442 2141–2144.
- 443 Haigh, J. D., Winning, A. R., Toumi, R., & Harder, J. W. (2010). An influence of  
444 solar spectral variations on radiative forcing of climate. *Nature*, 467(7316), 696–  
445 699. Retrieved from <http://dx.doi.org/10.1038/nature09426> doi: 10.1038/  
446 nature09426
- 447 Huang, Y., Xia, Y., & Tan, X. (2017). On the pattern of CO  
448 <sub>2</sub> radiative forcing and poleward energy transport. *Journal of*  
449 *Geophysical Research: Atmospheres*, 578–593.
- 450 Iacono, M. J., Delamere, J. S., Mlawer, E. J., Shephard, M. W., Clough, S. A., &  
451 Collins, W. D. (2008). Radiative forcing by long-lived greenhouse gases: Calcu-  
452 lations with the AER radiative transfer models. *Journal of Geophysical Research*  
453 *Atmospheres*, 113(13), 2–9. doi: 10.1029/2008JD009944
- 454 Irvine, P., Emanuel, K., He, J., Horowitz, L. W., Vecchi, G., & Keith, D. (2019).  
455 Halving warming with idealized solar geoengineering moderates key climate haz-  
456 ards. *Nature Climate Change*, 9(4), 295–299. doi: 10.1038/s41558-019-0398-8
- 457 Irvine, P. J., Kravitz, B., Lawrence, M. G., & Muri, H. (2016). An overview of the  
458 Earth system science of solar geoengineering. *Wiley Interdisciplinary Reviews: Cli-*  
459 *mate Change*, 7(6), 815–833. doi: 10.1002/wcc.423
- 460 Jeevanjee, N., & Roms, D. M. (2018). Mean precipitation change from a deepening  
461 troposphere. *Proceedings of the National Academy of Sciences*, 115(45), 11465–  
462 11470.
- 463 Keith, D. (2013). A case for climate engineering. *A Case for Climate Engineering*,  
464 1–199. doi: 10.7551/mitpress/9920.001.0001
- 465 Keith, D. W. (2010). Photophoretic levitation of engineered aerosols for geoengi-  
466 neering. *Proceedings of the National Academy of Sciences of the United States of*  
467 *America*, 107(38), 16428–16431. doi: 10.1073/pnas.1009519107
- 468 Khlebtsov, N. G., & Dykman, L. A. (2010). Optical properties and biomedical appli-  
469 cations of plasmonic nanoparticles. *Journal of Quantitative Spectroscopy and Ra-*  
470 *diative Transfer*, 111(1), 1–35. Retrieved from <http://dx.doi.org/10.1016/j>

- 471 .jqsrt.2009.07.012 doi: 10.1016/j.jqsrt.2009.07.012
- 472 Kleidon, A., Kravitz, B., & Renner, M. (2015). The hydrological sensitivity to global  
 473 warming and solar geoengineering derived from thermodynamic constraints. *Geo-*  
 474 *physical Research Letters*, *42*(1), 138–144. doi: 10.1002/2014GL062589
- 475 Kravitz, B., Caldeira, K., Boucher, O., Robock, A., Rasch, P. J., Alterskjær, K., ...  
 476 Yoon, J.-h. (2013). Climate model response from the Geoengineering Model Inter-  
 477 comparison Project ( GeoMIP ). *Journal of Geophysical Research: Atmospheres*,  
 478 *118*, 8320–8332. doi: 10.1002/jgrd.50646
- 479 Kravitz, B., Rasch, P. J., Forster, P. M., Andrews, T., Cole, J. N., Irvine, P. J., ...  
 480 Yoon, J. H. (2013). An energetic perspective on hydrological cycle changes in the  
 481 Geoengineering Model Intercomparison Project. *Journal of Geophysical Research*  
 482 *Atmospheres*, *118*(23), 13,087–13,102. doi: 10.1002/2013JD020502
- 483 Kravitz, B., Robock, A., Boucher, O., Schmidt, H., Taylor, K. E., Stenchikov, G., &  
 484 Schulz, M. (2011). The Geoengineering Model Intercomparison Project (GeoMIP).  
 485 *Atmospheric Science Letters*, *12*(2), 162–167. doi: 10.1002/asl.316
- 486 Krueger, S. K., Fu, Q., Liou, K. N., & Chin, H.-N. S. (1995, mar). Improvements of  
 487 an Ice-Phase Microphysics Parameterization for Use in Numerical Simulations of  
 488 Tropical Convection. *Journal of Applied Meteorology*, *34*, 281–287.
- 489 Lambert, F. H., & Faull, N. E. (2007). Tropospheric adjustment: The response  
 490 of two general circulation models to a change in insolation. *Geophysical Research*  
 491 *Letters*, *34*(3), 2–6. doi: 10.1029/2006GL028124
- 492 Lin, Y.-L., Farley, R. D., & Orville, H. D. (1983). *Bulk Parameterization of the*  
 493 *Snow Field in a Cloud Model* (Vol. 22) (No. 6).
- 494 Lord, S. J., Willoughby, H. E., & Piotrowicz, J. M. (1984, oct). Role of a Parameter-  
 495 ized Ice-Phase Microphysics in an Axisymmetric, Nonhydrostatic Tropical Cyclone  
 496 Model. *Journal of the Atmospheric Sciences*, *41*(19), 2836–2848.
- 497 Lutsko, N. J., Seeley, J. T., & Keith, D. W. (2020). Estimating Impacts and Trade-  
 498 offs in Solar Geoengineering Scenarios With a Moist Energy Balance Model. *Geo-*  
 499 *physical Research Letters*, *47*(9), 1–12. doi: 10.1029/2020GL087290
- 500 Niemeier, U., Schmidt, H., Alterskjær, K., & Kristjánsson, J. E. (2013). Solar  
 501 irradiance reduction via climate engineering: Impact of different techniques on  
 502 the energy balance and the hydrological cycle. *Journal of Geophysical Research*  
 503 *Atmospheres*, *118*(21), 11,905–11,917. doi: 10.1002/2013JD020445

- 504 O’Gorman, P. a., Allan, R. P., Byrne, M. P., & Previdi, M. (2011, nov). Energetic  
505 Constraints on Precipitation Under Climate Change. *Surveys in Geophysics*, 33(3-  
506 4), 585–608. doi: 10.1007/s10712-011-9159-6
- 507 Pendergrass, A. G., & Hartmann, D. L. (2014, jan). The Atmospheric Energy Con-  
508 straint on Global-Mean Precipitation Change. *Journal of Climate*, 27(2), 757–768.  
509 doi: 10.1175/JCLI-D-13-00163.1
- 510 Preston, C. J. (2013). Ethics and geoengineering: Reviewing the moral issues raised  
511 by solar radiation management and carbon dioxide removal. *Wiley Interdisci-  
512 plinary Reviews: Climate Change*, 4(1), 23–37. doi: 10.1002/wcc.198
- 513 Romps, D. M. (2008). The Dry-Entropy Budget of a Moist Atmosphere. *Journal of  
514 the Atmospheric Sciences*, 65(12), 3779–3799.
- 515 Romps, D. M. (2011). Response of Tropical Precipitation to Global Warming. *Jour-  
516 nal of the Atmospheric Sciences*, 68(1), 123–138.
- 517 Romps, D. M. (2014, oct). An Analytical Model for Tropical Relative Humidity.  
518 *Journal of Climate*, 27(19), 7432–7449.
- 519 Romps, D. M. (2020). Climate Sensitivity and the Direct Effect of Carbon Dioxide  
520 in a Limited-Area Cloud-Resolving Model. *Journal of Climate*, 33(9), 3413–3429.  
521 doi: 10.1175/jcli-d-19-0682.1
- 522 Romps, D. M., & Kuang, Z. (2010). Do Undiluted Convective Plumes Exist in the  
523 Upper Tropical Troposphere? *Journal of the Atmospheric Sciences*, 67, 468–484.
- 524 Seeley, J. T., Jeevanjee, N., Langhans, W., & Romps, D. M. (2019). Formation of  
525 Tropical Anvil Clouds by Slow Evaporation. *Geophysical Research Letters*, 46(1),  
526 492–501.
- 527 Seeley, J. T., Jeevanjee, N., & Romps, D. M. (2019). FAT or FiTT: Are anvil clouds  
528 or the tropopause temperature-invariant? *Geophysical Research Letters*, 46(3),  
529 1842–1850.
- 530 Seeley, J. T., & Romps, D. M. (2015). Why does tropical convective available poten-  
531 tial energy (CAPE) increase with warming? *Geophysical Research Letters*, 42(23),  
532 10429–10437.
- 533 Seeley, J. T., & Romps, D. M. (2016). Tropical cloud buoyancy is the same in a  
534 world with or without ice. *Geophysical Research Letters*, n/a—n/a.
- 535 Sherwood, S., Webb, M. J., Annan, J. D., Armour, K. C., Forster, P. M., Har-  
536 greaves, J. C., ... Zelinka, M. D. (2020). An assessment of Earth’s climate

- 537 sensitivity using multiple lines of evidence. *Reviews of Geophysics*, 1–166.
- 538 Sherwood, S. C., Bony, S., Boucher, O., Bretherton, C., Forster, P. M., Gregory,  
539 J. M., & Stevens, B. (2015). ADJUSTMENTS IN THE FORCING – FEEDBACK  
540 FRAMEWORK FOR UNDERSTANDING CLIMATE. *Bulletin of the American  
541 Meteorological Society*(February), 217–228. doi: 10.1175/BAMS-D-13-00167.1
- 542 Smith, C. J., Kramer, R. J., Myhre, G., Forster, P. M., Soden, B. J., Andrews, T.,  
543 ... Watson-Parris, D. (2018). Understanding Rapid Adjustments to Diverse  
544 Forcing Agents. *Geophysical Research Letters*, 45(21), 12,12–23,31.
- 545 Smyth, J. E., Russotto, R. D., & Storelvmo, T. (2017). Thermodynamic and dy-  
546 namic responses of the hydrological cycle to solar dimming. *Atmospheric Chem-  
547 istry and Physics*, 17(10), 6439–6453. doi: 10.5194/acp-17-6439-2017
- 548 Teller, E., Wood, L., & Hyde, R. (1997). *Global Warming and Ice Ages: I. Prospects  
549 for Physics-Based Modulation of Global Change*.
- 550 Tilmes, S., Fasullo, J., Lamarque, J.-f., Marsh, D. R., Mills, M., Alterskjær, K.,  
551 ... Niemeier, U. (2013). The hydrological impact of geoengineering in the Geo-  
552 engineering Model Intercomparison Project ( GeoMIP ). *Journal of Geophysical  
553 Research: Atmospheres*, 118, 36–58. doi: 10.1002/jgrd.50868